Stable and metastable phases of PTCDA on epitaxial NaCl films on Ag(100)

Eric Le Moal,* Mathias Müller, Oliver Bauer, and Moritz Sokolowski†
Institut für Physikalische und Theoretische Chemie, Universität Bonn, Wegelerstrasse 12, 53115 Bonn, Germany
(Received 16 December 2009; revised manuscript received 21 May 2010; published 1 July 2010)

Thin films of the model molecule perylene-3,4,9,10-tetracarboxylic acid dianhydride (PTCDA) were vacuum deposited on epitaxial NaCl films on Ag(100) and investigated by spot-profile-analysis low-energy electron diffraction (SPA-LEED). At growth temperatures between 193 K and room temperature (RT), the first layer (monolayer) exhibits a commensurate $(3\sqrt{2}\times 3\sqrt{2})R45°$ superstructure with a quadratic unit cell, which is identical to that found for PTCDA growth on bulk NaCl crystals [Burke *et al.*, Phys. Rev. Lett. **100**, 186104 (2008)]. At RT, dewetting occurs and complicates the formation of multilayers. However, at low surface temperatures (223 K), closed PTCDA multilayers grow. The corresponding unit cell [19.69(4) Å $\times$ 12.23(3) Å] is rectangular and similar to the herringbone structure of the (102) bulk plane of PTCDA. This growth form is metastable and the surface dewets upon annealing at 300 K. Submonolayers deposited at low temperatures (20–100 K) are disordered; upon annealing, they transform into the $(3\sqrt{2}\times 3\sqrt{2})R45°$ structure via a third metastable phase with a herringbone-type rectangular unit cell.

DOI: 10.1103/PhysRevB.82.045301 PACS number(s): 68.43.Hn, 68.55.am, 68.49.Jk

I. INTRODUCTION

Thin films of π-conjugated organic molecules have attracted much attention for their promising applications in optical and semiconducting devices.[1] Within this context, a number of surface-science experiments have been performed on the chemical interaction, the growth behavior, and the structural order of π-conjugated molecules on a large variety of surfaces.[2,3] Whereas investigations on metal substrates are rather straightforward, experiments on insulators as substrates are much more difficult because of two problems. First, charging effects limit the use of electron-based spectroscopies, and, second, due to the smaller molecule substrate interactions *Vollmer-Weber*-type growth is prevailing, which leads to incomplete wetting of the substrate and growth of small bulklike crystallites which are not well accessible by surface-science techniques, e.g., electron spectroscopies. Examples for the Vollmer-Weber growth are, e.g., perylene-3,4,9,10-tetracarboxylic acid dianhydride (PTCDA) (Ref. 4) and N,N′-dimethylperylene-3,4,9,10-bis(dicarboximide) deposited on the KBr(100) surface.[5]

Charging effects for electrons can be avoided by using thin epitaxial layers of insulators on semiconductors or metals as substrates. For instance, NaCl, KCl, and KBr can be deposited in the form of (100)-terminated layers on a number of metals as Cu,[6–12] Ag,[12–18] and Au.[19,20] These thin epitaxial films exhibit the chemical surface properties of the respective bulk insulators, but avoid charging effects, since the electrons can tunnel into the conducting underlying substrate.[21–26] Evidently, the spectroscopy of large organic molecules on insulator surfaces is highly interesting and complementary to that on metal surfaces. One reason is that, due to the weaker interactions with the substrate compared to metals substrates, the intrinsic molecular states and the intermolecular interactions are more dominant and can be hence studied. A second reason is the technological relevance of the organic/insulator interface, e.g., for organic field-effect transistors.[1] So far, mostly thin alkali-halide films on metals have been used for this purpose.[27–31] For instance, nearly unperturbed molecular orbitals were imaged successfully by scanning tunneling microscopy (STM) for pentacene,[26] Fe(II)-phthalocyanine,[32] and methylterrylene[33] on thin NaCl films on Cu(111).

The growth of the model molecule PTCDA has been investigated on the (100) cleavage surfaces of alkali-halide bulk crystals, namely, NaCl,[34–38] KCl,[35,36,38,39] and KBr (Refs. 4, 35, 38, and 40) by atomic force microscopy (AFM), and on thin KBr films on InSb(100) by STM.[30] In the present work, we report on the growth of PTCDA on thin epitaxial films of NaCl/Ag(100), which has not been investigated so far. We used spot-profile-analysis low-energy electron diffraction (SPA-LEED) (Ref. 41) which ensures that statistically correct data are obtained and allows to determine structural parameters with high precision.

Concerning the growth of PTCDA on NaCl(100) bulk crystals, Burke *et al.*[34] have recently reported the formation of PTCDA monolayer (ML) islands with a commensurate $p(3\times 3)$ superstructure in the submonolayer regime. Based on observations by noncontact AFM, the authors described a dewetting transition that occurs upon completion of the first closed monolayer and leads to the formation of bulklike PTCDA crystallites. This dewetting transition was ascribed to instability of the $p(3\times 3)$ superstructure of the monolayer with respect to additional PTCDA layers on top of it. Furthermore, on the basis of molecular mechanics calculations, the authors proposed that molecules in the first interfacial monolayer rearrange in a $p(2\times 3)$ superstructure, when being covered by a second layer. However, we found that at lower temperatures, this dewetting can be avoided and stable PTCDA multilayers coexist with the commensurate $p(3\times 3)$ structure on the time scale of the experiments. We further found that the multilayers exhibit an incommensurate structure that is very close to that of the herringbone (HB) arrangement in PTCDA bulk crystals. We will report on the details of these structures, the film growth, and the thermal stability of the PTCDA films as a function of film thickness and the substrate temperature during and subsequent to the growth.

II. EXPERIMENTAL DETAILS

All experiments were carried out in a UHV chamber at a base pressure of 3×10^{-10} mbar. The chamber is equipped with a SPA-LEED apparatus manufactured by Omicron NanoTechnology GmbH.[41] For deposition control, a mass spectrometer and a quartz microbalance were used. The sample was mounted on a manipulator cooled by either liquid helium or liquid nitrogen, making a temperature range of 20 K, respectively, 130–900 K accessible. All SPA-LEED data were typically collected at 34 eV electron energy at low-sample currents (~1 nA) in order to avoid charging effects, dissociation, or desorption of PTCDA molecules upon electron bombardment.

The preparation of the Ag(100) surface was performed as described in Ref. 42. NaCl and PTCDA were deposited by thermal evaporation from homemade Knudsen cells. The NaCl with 99.999% purity was purchased from Sigma-Aldrich. The PTCDA was purified by several cycles of gradient sublimation. The NaCl was deposited from a Knudsen cell at 700 K and at deposition rates of about 0.1–0.5 monolayers per minute (ML min^{-1}, for the exact definition of 1 ML see below) on the Ag(100) surface which was held at room temperature (RT, ≈300 K) or at 450 K. The NaCl films used in the present experiment had a thickness of about ten layers (corresponding to 29 Å). Notably, NaCl films on Ag(100) are not single crystalline but consist of domains which exhibit a small rotational mosaic spread of their [010] axes with respect to the [010] direction of Ag(100) substrate. This has been described recently in detail in Ref. 43.

For deposition of PTCDA, the cell temperature was about 700 K, yielding deposition rates of 0.05 ML min^{-1}. The sample temperatures were varied from 193 K to RT, except for the preparation of a disordered phase which was done at 100 K. Subsequent to the PTCDA deposition and prior to the SPA-LEED measurements, the sample was cooled down to 20 K by He cooling (or to 130 K by liquid nitrogen). Subsequent deliberate annealing steps consisted in heating the sample at a rate of 1 K s^{-1}, holding it at a specific temperature during the annealing time, and final cooling down to 20 K for further SPA-LEED measurements.

The nominal PTCDA film thickness will be given in numbers of monolayers. Hereby one monolayer (1 ML) is defined as the density of molecules in the (102) plane of the bulk β phase of PTCDA (8.32×10^{13} cm^{-2}).[44] The nominal thickness refers to the integral over the deposition flux that was measured by a mass spectrometer close to the Ag(100) sample. The calibration in number of ML was obtained from earlier deposition experiments on the bare Ag(100) surface, where the completion of the monolayer and the growth start of the second layer could be distinguished by different LEED patterns and by thermal desorption spectroscopy.[42] Evidently, this calibration assumes an identical and constant sticking probability.

III. RESULTS AND DISCUSSION

A. Quadratic monolayer structure

Figure 1(a) shows a typical SPA-LEED pattern of a thin PTCDA film of about 0.7 ML thickness, grown at 223 K.

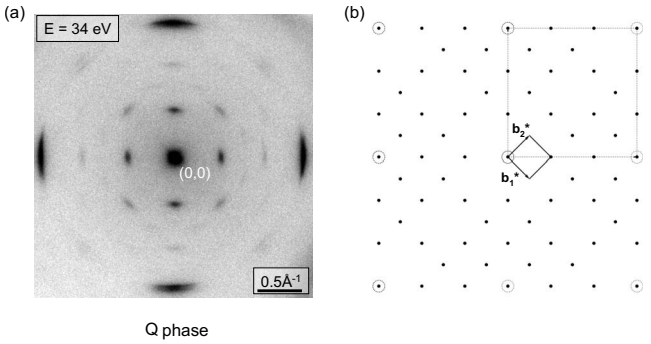

FIG. 1. (a) SPA-LEED pattern of a PTCDA film with a nominal thickness of about 0.7 ML, grown on a 10-ML-thick NaCl film on Ag(100) at 223 K. The electron energy was 34 eV. (b) Schematic presentation of the LEED pattern according to the structure model illustrated in Fig. 2(a). The reciprocal unit vectors $\mathbf{b}_1^*$ and $\mathbf{b}_2^*$ of the commensurate quadratic PTCDA structure are given, as well as the corresponding unit cell (solid line) and that of the NaCl(100) plane (dotted line).

The elongated shape of the NaCl spots is due to the above-noted rotational mosaicity of the NaCl film (so-called *azimuthal mosaicity*).[43] We find the NaCl and PTCDA spots to exhibit the same azimuthal broadening, which indicates that the PTCDA domains grow in a strict epitaxial relation with respect to the NaCl substrate without any additional observable rotational spread. In the radial direction the PTCDA spots are relatively sharper. Investigations on the radial width as a function of electron energy (not shown here) reveal that ordered PTCDA domains of about 150 Å in diameter have formed.

Remarkably, the SPA-LEED pattern in Fig. 1(a) is rather similar to that of a PTCDA monolayer directly grown on Ag(100).[42] In both cases, a quadratic structure and the same selective spot extinctions are observed (see below). On Ag(100), the PTCDA monolayer exhibits a commensurate $(4\sqrt{2}\times4\sqrt{2})R45°$ superstructure. On the thin NaCl films, we determine a commensurate $(3\sqrt{2}\times3\sqrt{2})R45°$ superstructure. Its basis vectors $\mathbf{b_1}$ and $\mathbf{b_2}$ are defined by the following matrix:

$$(\mathbf{b_1},\mathbf{b_2}) = \begin{pmatrix} 3 & 3 \\ -3 & 3 \end{pmatrix}(\mathbf{a_1},\mathbf{a_2}),$$

where $\mathbf{a_1}$ and $\mathbf{a_2}$ are the basis vectors of NaCl(100) surface, defining the primitive unit cell. Figure 1(b) shows the unit cell in reciprocal space. For this superstructure a quadratic unit cell with a lattice constant of 16.92 Å (at RT) is calculated, which is in good agreement with the value of 17.0 ± 0.1 Å directly determined by SPA-LEED.

The observed commensurate $(3\sqrt{2}\times3\sqrt{2})R45°$ superstructure is indeed identical to the structure noted as $p(3\times3)$ that was previously reported by Burke *et al.*[34] for PTCDA submonolayers on the bulk NaCl(100) surface. The two different notations result from different unit cells chosen for the NaCl(100) surface: Whereas we have denominated the adsorbate superstructure with respect to the primitive unit cell of NaCl(100) surface, Burke *et al.* referred to the larger centered unit cell rotated by 45° with respect to the primitive

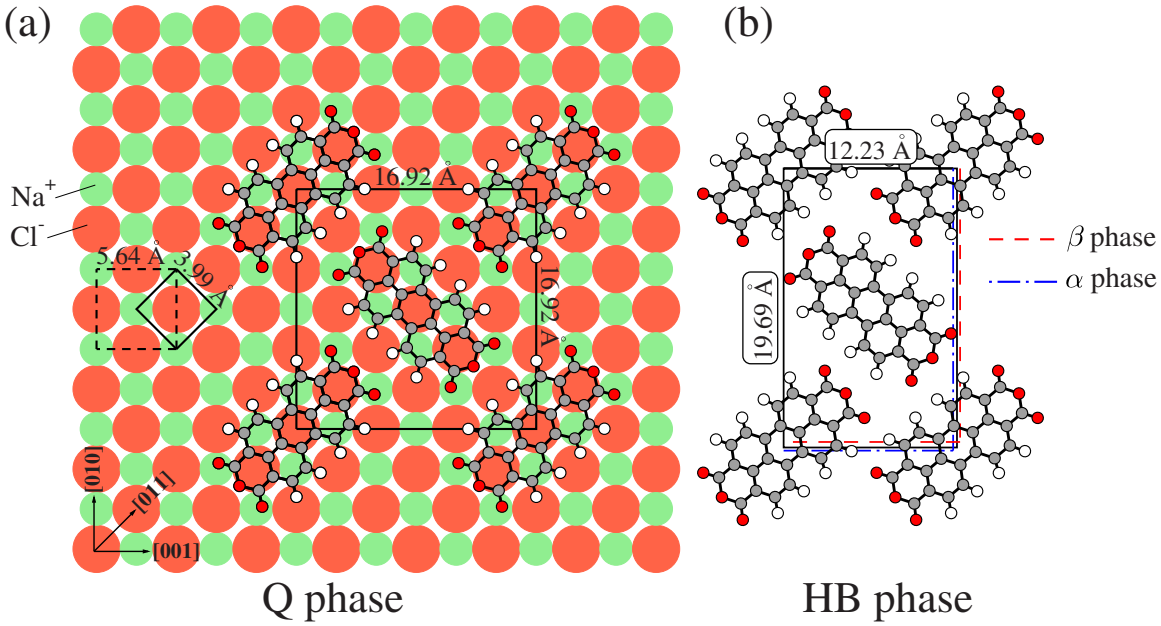

FIG. 2. (Color online) (a) Real-space structure model for the commensurate growth of the first PTCDA monolayer on NaCl(100). Large red spheres and small green spheres represent chlorine and sodium atoms, respectively. The main directions of the NaCl(100) plane are referred to as [010] and [001] with respect to the axes of the bulk fcc crystal. The centered unit cell (dashed black line) and the primitive unit cell (solid black line) of NaCl(100) are indicated with their dimensions at RT (Refs. 45 and 46). The unit cell of the commensurate quadratic PTCDA structure is marked (black line) with the dimensions defined by its relationship of commensurability with NaCl(100). (b) Real-space structure model of the incommensurate herringbone PTCDA structure in multilayered PTCDA films on NaCl(100). Its experimentally measured dimensions are indicated (19.69 Å × 12.23 Å). Its unit cell (solid black line) is compared to those of the (102) plane of the PTCDA bulk structure in the α (dashed-dotted blue line) and β phase (dashed red line).

unit cell [cf. Fig. 2(a)]. Figure 2(a) shows a corresponding structure model in real space. The systematic absences of the $(n,0)$ and $(0,k)$ spots, if n and k are odd numbers, indicate the presence of two glide planes (symmetry group $p4gm$). As for PTCDA on Ag(100), this in-plane symmetry is consistent with a so-called "T-shaped" arrangement of the molecules.[42] Within this model, PTCDA molecules lie flat on the NaCl films with their main axis along the NaCl [011] and [0$\bar{1}$1] directions and the primitive unit cell of the superstructure comprises two molecules perpendicularly oriented to each other.

The adsorption sites illustrated in Fig. 2(a) were chosen on the basis of considerations on energy minimization. The carbonyl oxygen atoms of PTCDA carry negative partial charges and hence presumably interact electrostatically with the sodium cations of the substrate surface. Burke *et al.*[34] have demonstrated by molecular mechanics and density-functional calculations that these attractive forces are responsible for the in-plane molecular arrangement and the orientation of the first PTCDA monolayer on NaCl(100). An analog conclusion was drawn by Dienel *et al.*[39] for PTCDA on KCl(100) from molecular force-field calculations. Interestingly, the resulting arrangement of PTCDA on NaCl(100) [see Fig. 2(a)] provides equivalent adsorption sites for all eight carbonyl oxygen atoms within the unit cell. From now on, we refer to this commensurate quadratic PTCDA structure as the *Q phase*. Notably, this Q phase differs considerably from the denser herringbone packing of PTCDA that is found in the (102) plane of bulk crystals (see Table I) (Refs. 44 and 47) and that is typical for PTCDA adsorbed on weakly interacting surfaces, e.g., Au(111).[48] The molecular density within the Q phase (6.99×10^{13} cm^{-2}) is about 16% lower compared to that found in the (102) plane of the bulk β phase of PTCDA (8.32×10^{13} cm^{-2}). The commensurability and the lower density of the Q phase both reflect that rather strong interactions between the PTCDA and the NaCl surface exist.

B. Herringbone structure of the multilayers

Figure 3 shows two LEED patterns of a PTCDA film of about 2.7 ML in nominal thickness, grown at 223 K. The pattern in Fig. 3(a) was measured directly after growth and cooling to 20 K while that in Fig. 3(b) was recorded after additional annealing at 300 K for 72 h and cooling to 20 K. In addition to the Q phase, an *incommensurate* PTCDA superstructure is observed in Fig. 3(a). It exhibits a rectangular unit cell with unit vectors ($\mathbf{c_1}$ and $\mathbf{c_2}$) parallel to those of the Q phase ($\mathbf{b_1}$ and $\mathbf{b_2}$). As expected, there are two symmetry equivalent domains, rotated by 90° relative to each other. Hence we conclude that from the second layer onward PTCDA nucleates with a different lateral packing on top of the first monolayer. The LEED spots from the Q phase in Fig. 3(a) could be interpreted as stemming either from uncovered areas of the monolayer due to a partial Stranski-Krastanov growth type, or from regions where the monolayer is covered by further layers, but still exhibits the order of the Q phase and contributes to the scattered intensity due to the

TABLE I. Structural parameters of the unit cells of different PTCDA phases on epitaxial NaCl films on Ag(100). There are two monolayer phases [quadratic (Q) and herringbone (HB*)] and a herringbone-type multilayer phase (HB). For comparison, the unit cells of the (102) planes of the respective bulk phases of PTCDA are given (Ref. 44).

	Q phase (monolayer) commensurate	HB* phase (monolayer) incommensurate	HB phase (multilayer) incommensurate	Bulk α phase (102) plane	Bulk β phase (102) plane
Length of unit vectors (Å)	$b_1=16.92$	$d_1=20.2\pm0.2$	$c_1=19.69\pm0.04$	19.91	19.30
	$b_2=16.92$	$d_2=13.5\pm0.1$	$c_2=12.23\pm0.03$	11.96	12.45
Angle between the unit vectors (deg)	90	90	90	90	90
Orientation with respect to the unit cell of the substrate (deg)	45	45	45		
Unit-cell area (Å^2)	286.3	272 ± 3	241 ± 1	238.1	240.3

penetration of the electrons through the uppermost layers.

Assuming a perfect commensurability of the Q phase, we used its diffraction pattern as a reference to determine the lattice parameters of the multilayer phase with high precision. Figure 4 shows radial scans, measured along the $[1\bar{1}]$ direction before (*black dots*) and after annealing (*blue triangles*), exactly under the same experimental conditions as those of Figs. 3(a) and 3(b). Diffraction spots from the Q phase and the multilayers are observed along this scan direction. Their positions were determined by fitting the peaks with a set of Lorentzians (see Fig. 4). The so determined rectangular unit cell exhibits the parameters: $c_1=19.69\pm0.04$ Å and $c_2=12.23\pm0.03$ Å. It is described by the following matrix:

$$(\mathbf{c_1},\mathbf{c_2}) = \begin{pmatrix} 3.491\pm0.007 & 3.491\pm0.007 \\ -2.168\pm0.005 & 2.168\pm0.005 \end{pmatrix} (\mathbf{a_1},\mathbf{a_2}),$$

where $(\mathbf{c_1},\mathbf{c_2})$ and $(\mathbf{a_1},\mathbf{a_2})$ are the basis vectors of the PTCDA superstructure and those of the NaCl surface, respectively. The dimensions of the unit cell of the multilayer phase unit are very close, although *not* identical, to those of

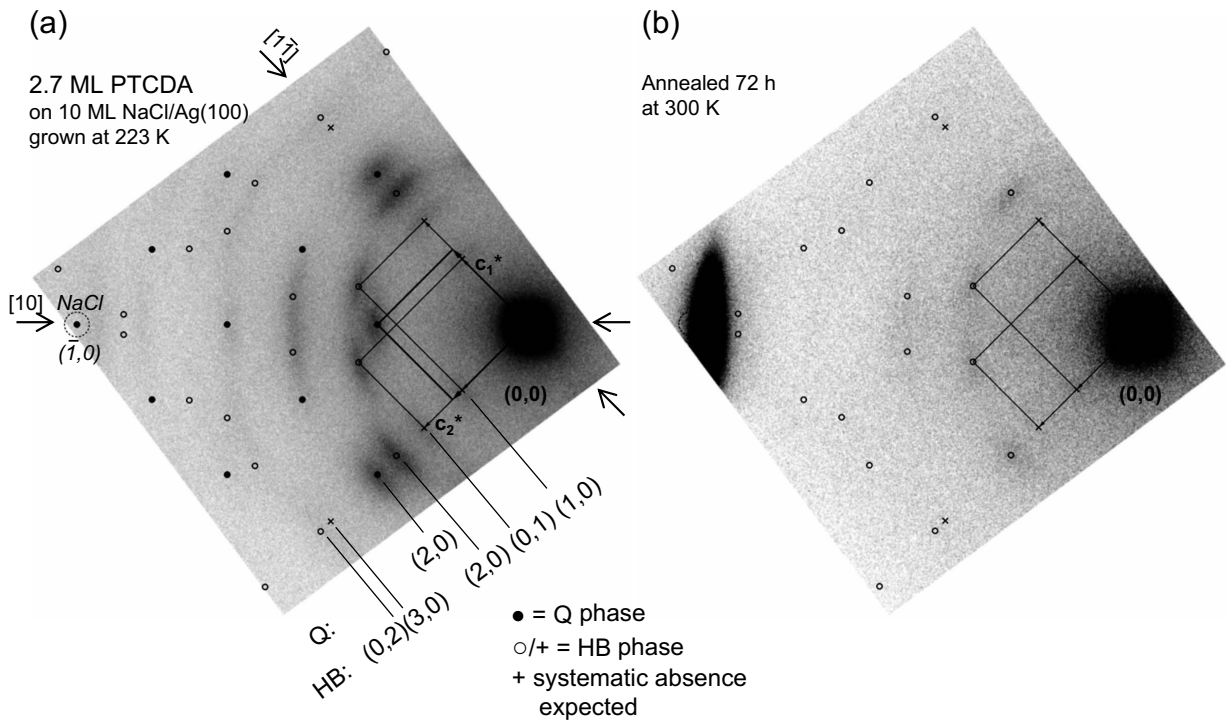

FIG. 3. SPA-LEED patterns of a multilayer PTCDA film with about 2.7 ML in nominal thickness, grown on a 10-ML-thick NaCl film on Ag(100) at 223 K. (a) just after growth and (b) after annealing at 300 K for 72 h. In the superimposed simulations of LEED pattern, the full circles and bold arrows represent the diffraction spots and the reciprocal unit vectors ($\mathbf{b_1^*}$ and $\mathbf{b_2^*}$) of the commensurate PTCDA structure (Q phase). The empty circles and thin arrows represent the diffraction spots and the reciprocal unit vectors ($\mathbf{c_1^*}$ and $\mathbf{c_2^*}$) of the incommensurate PTCDA structure (HB phase). The crosses indicate the $(n,0)$ and $(0,k)$ spots of the incommensurate PTCDA structure where n and k are odd numbers, which are expected to be absent in the presence of two glide planes. A dashed circle on the left side of the LEED patterns indicates the position of the NaCl $(\bar{1},0)$ spot. [10] and $[1\bar{1}]$ are the substrate directions along which the spot profiles were measured.

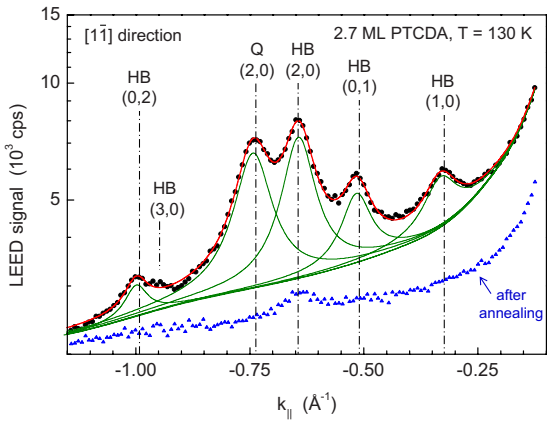

FIG. 4. (Color online) Radial SPA-LEED profiles, measured along the [1$\bar{1}$] direction of Fig. 3(a) (black dots) and Fig. 3(b) (blue triangles) under the same conditions of observation. Spots from both the commensurate (Q) and incommensurate (HB) PTCDA structures are observed along this direction. The exact positions of the diffraction spots were determined by fitting the profiles with a set of Lorentzian peaks (*green curves and red envelope*).

the unit cell of the [102] plane of the β phase (19.30 Å $\times$12.45 Å) or the α phase (19.91 Å$\times$11.96 Å) of PTCDA bulk crystals[44] [see Table I and Fig. 2(b)]. However, within error the unit cell exhibits the same area (241 ± 1 Å^2) as the unit cell of the (102) plane of the β phase bulk structure (240.3 Å^2). The corresponding in plane molecular density is calculated at 8.3×10^{13} cm^{-2}. It is hence plausible that the molecules arrange with a herringbone packing very similar to that within the (102) bulk plane. Hence the multilayer structure is referred to as the HB phase in the following. It differs from the $p(2\times3)$ structure that was proposed by Burke *et al.*,[34] and which exhibits a smaller unit cell.

In the (102) plane of the PTCDA bulk phase, the herringbone arrangement with two molecules per unit cell implies two glide planes (symmetry group $p2gg$). Hence, systematic absences of the $(n,0)$ and $(0,k)$ spots if n and k are odd numbers are expected. These spots are marked by crosses in Fig. 3(a). However, the (0,1) and (1,0) spots of the HB phase can be clearly seen in the LEED scan displayed in Fig. 4. Two explanations can be envisaged: multiple-scattering effects, which involve the underlying PTCDA layers and/or a possible deviation from the $p2gg$ symmetry.

C. Stability and growth mode of the multilayers

1. Thermal stability of the multilayers

As demonstrated in Figs. 3 and 4, the annealing of the PTCDA film yields an overall fading of the LEED pattern. A structural transition is identified from the comparison of the LEED patterns prior to and after annealing. This transition has to be compared to the dewetting transition at RT previously reported by Burke *et al.*[34]

Directly after PTCDA growth at 223 K, the LEED pattern is dominated by the intense (2,0), (0,2), and (1,1) spots of the Q and HB phases [see Fig. 3(a)]. After annealing at 300 K for 72 h, only the spots of the HB phase can be detected, however, with much lower intensity [see Figs. 3(b) and 4]. Prior to the annealing, the (2,0) spots of both PTCDA structures exhibited roughly the same intensity but afterwards only those of the HB phase can be seen (*blue triangular data points in Fig. 4*). In addition, the intensity of the $(\bar{1},0)$ spot of the underlying NaCl film that was almost completely damped prior annealing, raised by several orders of magnitude during annealing [see Fig. 3(b)].

These results are interpreted by a dewetting of the substrate during the annealing. Desorption of PTCDA can be excluded at this temperature. Prior to annealing, HB-ordered layers exist on top of a closed first monolayer. After annealing, multilayer islands (crystallites) with HB structure have formed, leaving the bare NaCl surface in between these. We note that the multilayer islands yield only weak LEED spots due to their small surface coverage. From our data we cannot discriminate unambiguously whether the first layer below the multilayer islands maintains in the Q phase or transforms into the HB structure during the dewetting. This *temperature-induced* dewetting is compatible to the *coverage-induced* dewetting that was observed at RT at a coverage close to the completion of the monolayer by Burke *et al.*[49] We note that the dewetting occurs faster at higher annealing temperatures. For example, we found that a short annealing at 327 K for 5 min yields a comparable change in the LEED pattern as described above for annealing at RT.

2. Multilayer growth

We now turn to the growth at low temperatures in more detail. Figure 5 shows radial SPA-LEED profiles of PTCDA films ranging from 0.14 to 1.85 ML in nominal thickness, all grown at 223 K sample temperature. All spot profiles were measured along the [10] direction (cf. Fig. 3) after cooling the sample to 130 K. According to the in-plane molecular densities of the Q and HB phases, an ideal layer-by-layer growth would yield a closed monolayer of the Q phase at a nominal thickness of 0.85 ML, and the second closed layer (HB phase) at 1.85 ML. (Note that 1 ML corresponds to the density of the HB phase.) Following observations can be made from Fig. 5: (i) the NaCl $(\pm1,0)$ spots gradually diminish in intensity with increasing nominal film thickness, as it is principally expected for a layer-by-layer growth. However, the existence of some open layers may be still possible. (ii) There are no indications for a dewetting upon completion of the monolayer at 0.85 ML since this would otherwise cause a strong increase in intensity of the NaCl $(\pm1,0)$ spots. (iii) The spots of the Q phase increase in intensity up to 0.85 ML and decrease for higher nominal film thickness. This is consistent with a growth scenario, where the HB phase overgrows the Q phase ordered monolayer and attenuates the intensity of the electrons diffracted from the monolayer. This situation that the Q phase is preserved in the first interfacial layer after it has been overgrown is most conceivable.

However, a structural transition of the "buried" monolayer from the Q to the HB phase would be also compatible with the data. In this case, the diffracted Q phase intensity would stem from open (i.e., uncovered) areas of the monolayer. So far an unambiguous discrimination between both scenarios is

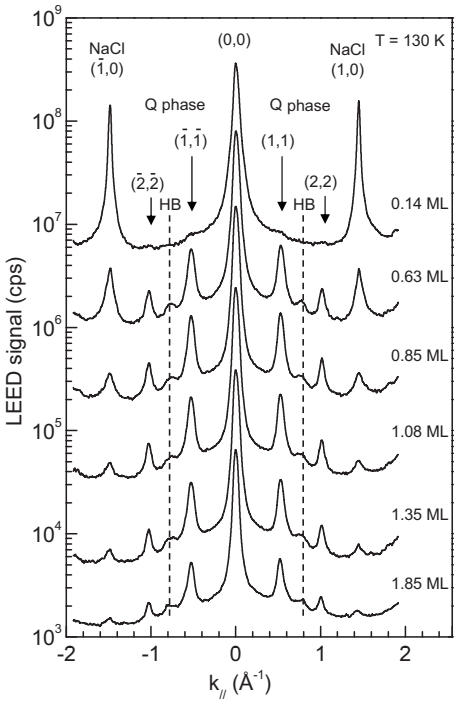

FIG. 5. Radial SPA-LEED profiles of PTCDA films ranging from 0.14 to 1.85 ML in nominal thickness, grown on a 10-ML-thick NaCl film on Ag(100) at 223 K, measured along the [10] direction under identical experimental conditions at a sample temperature of 130 K.

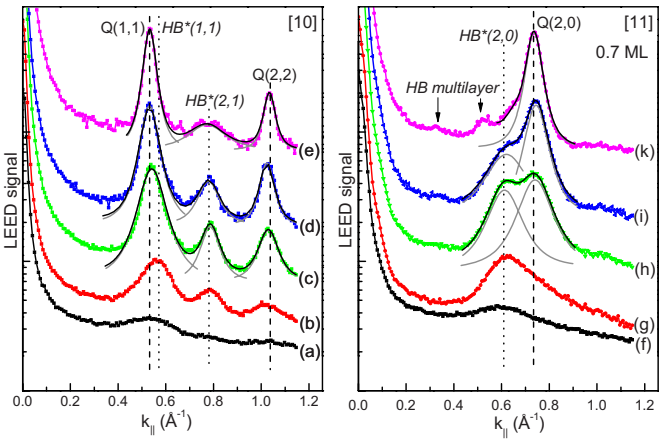

FIG. 6. (Color online) Radial SPA-LEED profiles of a thin PTCDA film of about 0.7 ML nominal thickness, grown on a 10-ML-thick NaCl film on Ag(100) at 100 K. Profiles (a)–(e) and (f)–(k) were measured along the [10] and [1$\bar{1}$] direction, respectively. Profiles (a) and (f) were measured directly after growth. The other profiles demonstrate the evolution after consecutive annealing. In detail: [(b) and (g)] after annealing at 200 K for 10 min, [(c) and (h)] after further annealing at 270 K for 15 min, [(d) and (i)] after further annealing at 270 K for 10 min and at 285 K for 10 min, [(e) and (k)] after further annealing at 285 K for 30 min and at 300 K for 20 min. The profiles are vertically shifted for clarity. The gray curves show individual peaks fitted to the data, the black curves are the sums of these. In order to avoid overloading, not all fitted components are shown. Note that spots from both the Q and the HB* structures are observed along both directions. For further details see text.

difficult. It can be expected that a Q to HB phase transition of the monolayer upon overgrowth would induce significant disorder in the second and higher layers, in particular, line defects, which would cause a broadening of the LEED spots. Since this is not observed, we favor the former scenario, i.e., the absence of the Q to HB phase transition. However, the formation of any other ordered structure than the Q or HB phase, e.g., the $p(2\times3)$ structure proposed by Burke *et al.* can be outruled since, due to the penetration depth of the diffracted electrons, this would lead to additional diffraction spots from the buried interfacial layer, which were not observed. We expect that the sensitivity of our LEED experiment would allow to detect the $p(2\times3)$ LEED spots, if about 10% of the interfacial structure would have ordered in this phase.

(iv) A small additional peak is observed between the (1,1) and (2,2) spots of the Q phase. For thickness below 0.85 ML this peak is the (2,0) spot of the Q phase grown on 45°-oriented NaCl domains, which is at $k_{\|}\approx0.74$ Å^{-1} along the [10] direction. For higher coverage the peak stems from the (2,1) spot of the HB phase (expected at $k_{\|}\approx0.82$ Å^{-1}). This spot does not fall exactly onto the [10] direction [see Fig. 3(a)] but can be seen along this scan direction due to its azimuthal broadening caused by the substrate [cf. Fig. 3(a)]. Its presence indicates the HB structure.

D. Transient formation of a herringbone structure in the monolayer

Remarkably, ordering of the molecules in a herringbone-type structure, which we call HB*, can also be achieved for the first monolayer under special conditions, namely, deposition at low temperatures and ordering of the disordered film by gradual annealing. A corresponding experiment is shown in Fig. 6. There we deposited 0.7 ML of PTCDA at 100 K. Figure 6 shows radial spot profiles measured along the [10] and [1$\bar{1}$] directions directly after the deposition [(a) and (f)] and after subsequent annealing steps. (For the details refer to the caption of Fig. 6.)

For the as-grown film, there are only weak and rather broad diffraction spots. This demonstrates that at 100 K the mobility of PTCDA on the NaCl surface is too small for ordering. Annealing at 200 K induces ordering of the PTCDA molecules and formation of ordered PTCDA domains, as evidenced by the diffraction spots in the scans (b) and (g). The strong asymmetry of the diffraction spots in scan (g) reveals that domains of the HB* and the Q phase have formed with a dominant contribution of the HB* phase. Annealing the sample further at temperatures between 270 and 300 K improves the structural order and spots of both the Q and the HB* phase can be clearly seen [see scans (c) and (h)]. Upon further annealing, the Q phase grows at the expense of the HB* phase, and after a number of annealing cycles, the relative contribution of the HB* phase is strongly reduced, as seen in scans (e) and (k). Hence, the HB* phase forms as a metastable phase when the molecules in the monolayer order. It coexists with the Q phase, which is apparently the most stable monolayer phase. When both phases coexist, the respective domain sizes are both rather small

(about 50–100 Å), as evidenced from the large full width at half maximum (FWHM) of the respective spots. From LEED alone it is difficult to quantify the ratio of the HB* to the Q phase. From independent photoluminescence data, we reckon that it amounts to 75–25 % at the most.[50] However, upon further annealing the Q phase spots increase and sharpen. For example, in Fig. 6, we see a reduction in the FWHM of the (2,0) and (2,2) spots of the Q phase by a factor of about 2 between the scans (b)/(g) and (e)/(k). For the (1,1) spot of the Q phase the spot sharpening is also observable, but due to the superposition with the (1,1) spots of the HB* phase, the quantification is difficult.

In conclusion, we find that upon starting from a disordered phase, the HB* phase forms in parallel with the Q phase but with a higher relative fraction. It gradually disappears, if stronger molecular diffusion is allowed, thus leading to the dominant and more stable Q phase. We note that from photoluminescence data taken on these films it can be independently verified that the HB* and the Q phase are different *monolayer* phases and that the HB phase is a *multilayer* phase.[50] As a result, in the monolayer, the HB* phase exists only as a transient phase under conditions where ordering into the Q phase is kinetically limited. Notably, the structural order in the HB* phase is rather limited, as seen from the rather broad peaks, and the observation that only LEED spots of lower order (up to 5) can be observed. However, if only a very small coverage of 0.15 ML is deposited, the HB*-ordered domains are not formed but ordering yields directly the Q phase. This indicates that a higher surface coverage that supports a large number of intermolecular contacts is essential for the formation of the HB* phase.

From a detailed peak analysis, we determined the lattice constants of the HB* phase in the monolayer. They are compiled in Table I. The corresponding matrix is

$$(\mathbf{d_1},\mathbf{d_2}) = \begin{pmatrix} 3.58 \pm 0.04 & 3.58 \pm 0.04 \\ -2.39 \pm 0.02 & 2.39 \pm 0.02 \end{pmatrix} (\mathbf{a_1},\mathbf{a_2}).$$

Notably the lattice constants differ from those of the HB arrangement in the multilayers; hence we denominate this structure HB*. Its unit cell is expanded by about 12% with respect to unit cell of the multilayer HB phase. The difference is likely due to the presence of the NaCl substrate. However, in contrast to the Q structure, the HB* structure is incommensurate. We note that the difference in the lattice constants can directly be seen in Fig. 6 in the profile (k), where due to the annealing faint (1,0) and (0,1) spots of the HB phase are seen, whereas the (2,0) spot of the HB* phase is no longer observable. Interestingly, the (0,1) and (1,0) spots of the HB* phase appear to be systematically absent as one would expect from symmetry considerations, i.e., the existence of glide planes as noted above.

IV. CONCLUDING DISCUSSION

The occurrence of the two different monolayer structures and different growth scenarios on NaCl(100) has to be understood as a consequence of the interplay of both energetic and kinetic aspects. In the monolayer, the Q phase is energetically favored over the HB* structure due to substrate-adsorbate interactions. These are presumably rather strong attractive electrostatic interactions between the Na^+ ions and negatively charged oxygen containing anhydride groups. They overbalance the intermolecular interactions, which would otherwise favor a herringbone arrangement of the molecules. In particular, the herringbone arrangement allows interactions between the anhydride groups and the H atoms on the periphery of the perylene cores.[51]

Evidently, the interaction between the PTCDA molecules in the monolayer and the second layer is too weak to transfer the quadratic order of the Q phase to the second layer, which consequently orders in the HB arrangement. However, the directions of the unit-cell vectors of the monolayer and the second layer coincide, indicating a mechanism of minimizing the interfacial energy between the first and second layer. As noted in the result section, the possibility of a transition of the Q phase into the HB phase upon overgrowth cannot strictly be outruled on the basis of our data. From an energetic point of view, this transition would require that the energy gain at the monolayer to second layer interface would overcompensate the loss in the adsorbate substrate interaction of the monolayer. This energetic difference is likely very small. A further experimental verification of the one or the other situation possibly requires the use of a localized structural method, e.g., STM.

Notably, the discussed growth scenario of PTCDA on NaCl(100) is analog to that of PTCDA on Ag(100).[42] On Ag(100), also a commensurate quadratic structure with a T-shaped arrangement of the molecules is formed in the monolayer. This structure has a unit cell ($b_1=b_2=16.34$ Å) that is by about 7% smaller compared to that of the Q phase on NaCl(100) ($b_1=b_2=16.92$ Å). However, as on NaCl(100), the second PTCDA layer on Ag(100) orders in a herringbone structure and exhibits almost the same lattice constants ($b_1=19.8$ Å and $b_2=12.2$ Å). Notably, for this system the presence of the T-shaped arrangement in the buried monolayer could be proved by STM.[42] Given that this scenario is also correct for PTCDA/NaCl(100), the misfit plane, where the lateral order relaxes to that of the bulk, is situated between the monolayer and the second layer in both systems.

However, there also exists an important difference between the two systems. Whereas the monolayer on Ag(100) is stable at elevated temperatures, it dewets from the NaCl(100) surface. This appears to be a consequence of the considerably stronger adsorption energy of PTCDA on Ag(100) compared to NaCl(100). In addition, the dewetting on NaCl reveals that the cohesive energy of the PTCDA crystal phase is larger than the adsorption energy of the molecule in the monolayer on NaCl. The observation of multilayer growth on NaCl(100) at reduced temperatures is hence clearly related to kinetic barriers which prevent the spontaneous dewetting and crystallite formation.

The formation of domains with a herringbone arrangement (HB*) in the monolayer on NaCl(100) under certain preparation conditions is also most interesting in this context. If this structure forms, the adsorbate-adsorbate interactions, which favor this structure dominate over the adsorbate-substrate interactions, which favor the more stable Q phase. This demonstrates how delicate the balance between the two

interactions in the monolayer is. We speculate that the formation of the long-range ordered Q phase requires more collective processes and possibly also the passing of a higher activation barrier than it is the case for the formation of the HB* phase. Hence, starting from a disordered phase, the HB* phase is formed predominantly, but only as a transient phase. This scenario is also supported by the fact that relatively small domains of the HB* phase are formed. So far, we have not been able to prepare the HB* phase as a pure phase but only together with some fraction of the Q phase.

We have to discuss our findings in relation with those of Burke *et al.*[34] on PTCDA on bulk NaCl. In general, our results are compatible with those of Burke *et al.* However, there are several points where we can amend these. First of all, we find that the spontaneous dewetting of the monolayer phase at room temperature is a temperature-driven process, which is, however, *not* present at low temperatures. Furthermore, Burke *et al.* have suggested on the basis of molecular mechanics calculations that the Q phase cannot be overgrown by a second layer but that it transforms into a $p(2\times3)$ structure (11.28 Å $\times$ 16.92 Å) when being covered by a second layer of PTCDA.[34] From our data we cannot support the transformation of the Q phase upon further deposition into a $p(2\times3)$ structure. As noted, this would cause additional (2×3) diffraction spot, which we do not observe. Notably, the $p(2\times3)$ is significantly compressed along its long axis with respect to the bulk HB arrangement ($\sim$16% and 13% for the α and β phase, respectively), leading to a small unit cell (only 80% of that of the HB phase). This implies a tilted (nonplanar) arrangement of the PTCDA molecules,[34] which we consider as unfavorable, since the system would lose considerably interaction energy between the substrate and the adsorbate. The only transformation of the buried monolayer, which is compatible with our data, would be that into the HB structure. Any other ordered structure would lead to corresponding additional LEED spots, which were not observed.

In a further publication Burke *et al.*[52] reported the formation of a $p(2\times4)$ structure (11.28 Å $\times$ 22.56 Å) within small pits on an NaCl(100) surface that was treated by charge irradiation before. This structure is well compatible with the space requirements of flat-lying PTCDA molecules. However, our data give no indications of the existence of this structure, possibly because it only forms in step-confined pits.

PTCDA monolayers were also studied on the KCl(100) (Ref. 39) and KBr(100) (Ref. 4) surface, which exhibit slightly larger lattice constants compared to NaCl(100) [a_{NaCl}=3.99 Å, a_{KCl}=4.45 Å, and a_{KBr}=4.67 Å (Ref. 45)]. In contrast to the situation on NaCl(100), a commensurate "brick-wall" arrangement of the molecules with a square-shaped unit cell (158.76 Å^2) with one molecule per cell is formed on KCl(100). The origin of this structure appears to be again an electrostatic interaction between the anhydride groups and the K^+ cations of the surface, however, favoring a different structure compared to NaCl(100). On KBr(100), an HB arrangement as in the bulk (α or β phase) is found. Possibly the lattice constant does not allow a commensurate structure with favorable electrostatic interaction to the substrate, and as a consequence, the intermolecular interactions order the molecules into the bulk structure. In summary, all these findings indicate a delicate balance between the substrate-adsorbate and the adsorbate-adsorbate interactions for PTCDA on different alkali-halide (100) surfaces and that the variations in the lattice constants and possibly also the presence of specific surface defects, e.g., steps, decide whether one or the other structure is energetically favored.

As noted at the beginning, thicker films of PTCDA on NaCl(100) were studied in the past by several groups[36,38] and show the presence of azimuthally aligned nanocrystallites. So far, we have not been able to understand these azimuthal orientations on the basis of the HB multilayer phase, which we observed. It may be hence that the orientation of the nanocrystals is strongly related to surface defects, as, for instance, steps.

Finally, we note that the closed and highly ordered monolayer of PTCDA on thin epitaxial NaCl constitutes an ideal system to study the intermolecular interactions in an extended two-dimensional organic film by surface-sensitive probes involving electrons, since charging effects, present on bulk NaCl(100), are avoided. The presence of differently ordered structures makes this system especially interesting, notably for investigating correlations between the intermolecular structural order and electronic and/or optical properties of ultrathin organic films.

V. SUMMARY

In the monolayer regime, PTCDA on thin NaCl films forms ordered domains with a commensurate $(3\sqrt{2}\times3\sqrt{2})R45°$ superstructure and a "T-shape" in-plane molecular arrangement. At suitable low temperatures (e.g., 223 K) the commensurate monolayer can be overgrown by well-ordered multilayers with a herringbone and hence bulk-like arrangement. At low temperatures, these multilayers are stable at the time scale of the observations. At RT, the PTCDA multilayers undergo a slow dewetting transition, which leaves most of the NaCl surface bare. Remarkably, a herribone arrangement with slightly modified lattice constants is observed as a transient phase for monolayers, if a disordered PTCDA film of nearly monolayer coverage grown at low temperatures (20–100 K) is ordered by annealing.

ACKNOWLEDGMENTS

We thank J. Ikonomov for discussion and help in simulating LEED patterns. This project was supported by the Deutsche Forschungsgemeinschaft through the Research Unit 557 "Light Confinement and Control with Structured Dielectrics and Metals." One of the authors (E.L.M.) acknowledges financing by the Alexander von Humboldt Foundation.

*Present address: Institut Fresnel (CNRS UMR 6133), Campus Universitaire de Saint-Jérôme, 13397 Marseille Cedex 20, France.
†Corresponding author. FAX: +49 (0)228-73 2551; sokolowski@pc.uni-bonn.de

[1] H. Klauk, *Organic Electronics* (Wiley-VCH, Weinheim, 2006).
[2] F. Rosei, M. Schunack, Y. Naitoh, P. Jiang, A. Gourdon, E. Laegsgaard, I. Stensgaard, C. Joachim, and F. Besenbacher, Prog. Surf. Sci. **71**, 95 (2003).
[3] G. Witte and C. Wöll, J. Mater. Res. **19**, 1889 (2004).
[4] T. Kunstmann, A. Schlarb, M. Fendrich, T. Wagner, R. Möller, and R. Hoffmann, Phys. Rev. B **71**, 121403 (2005).
[5] M. Fendrich and T. Kunstmann, Appl. Phys. Lett. **91**, 023101 (2007).
[6] R. Bennewitz, V. Barwich, M. Bammerlin, C. Loppacher, M. Guggisberg, A. Baratoff, E. Meyer, and H. J. Güntherodt, Surf. Sci. **438**, 289 (1999).
[7] R. Bennewitz, A. S. Foster, L. N. Kantorovich, M. Bammerlin, C. Loppacher, S. Schär, M. Guggisberg, E. Meyer, and A. L. Shluger, Phys. Rev. B **62**, 2074 (2000).
[8] T. Filleter, W. Paul, and R. Bennewitz, Phys. Rev. B **77**, 035430 (2008).
[9] A. Kikas, V. Kisand, T. Käämbre, R. Ruus, E. Nõmmiste, M. Hirsimäki, M. Valden, E. Kukk, H. Aksela, and S. Aksela, Surf. Sci. **584**, 49 (2005).
[10] A. Riemann, S. Fölsch, and K. H. Rieder, Phys. Rev. B **72**, 125423 (2005).
[11] M. Kiguchi, S. Entani, K. Saiki, H. Inoue, and A. Koma, Phys. Rev. B **66**, 155424 (2002).
[12] M. Kiguchi, Bull. Chem. Soc. Jpn. **80**, 637 (2007).
[13] K. F. Braun, D. Farias, S. Fölsch, and K. H. Rieder, Surf. Sci. **454-456**, 750 (2000).
[14] D. Farías, K. F. Braun, S. Fölsch, G. Meyer, and K. H. Rieder, Surf. Sci. **470**, L93 (2000).
[15] M. Kiguchi, T. Goto, K. Saiki, T. Sasaki, Y. Iwasawa, and A. Koma, Surf. Sci. **512**, 97 (2002).
[16] M. Pivetta, F. Patthey, M. Stengel, A. Baldereschi, and W.-D. Schneider, Phys. Rev. B **72**, 115404 (2005).
[17] J. Kramer, C. Tegenkamp, and H. Pfnür, J. Phys.: Condens. Matter **15**, 6473 (2003).
[18] K. Aït-Mansour, M. Bielmann, O. Gröning, P. Ruffieux, R. Fasel, and P. Gröning, Appl. Surf. Sci. **252**, 6368 (2006).
[19] F. Reniers, D. H. Fairbrother, S. Wu, and J. Lipkowski, Surf. Sci. **433-435**, 12 (1999).
[20] C. Loppacher, U. Zerweck, and L. M. Eng, Nanotechnology **15**, S9 (2004).
[21] U. Barjenbruch, S. Fölsch, and M. Henzler, Surf. Sci. **211-212**, 749 (1989).
[22] S. Fölsch, U. Barjenbruch, and M. Henzler, Thin Solid Films **172**, 123 (1989).
[23] K. Glöckler, M. Sokolowski, A. Soukopp, and E. Umbach, Phys. Rev. B **54**, 7705 (1996).
[24] W. Hebenstreit, J. Redinger, Z. Horozova, M. Schmid, R. Podloucky, and P. Varga, Surf. Sci. **424**, L321 (1999).
[25] R. Bennewitz, J. Phys.: Condens. Matter **18**, R417 (2006).
[26] J. Repp, G. Meyer, S. M. Stojković, A. Gourdon, and C. Joachim, Phys. Rev. Lett. **94**, 026803 (2005).
[27] L. Ramoino, M. von Arx, S. Schintke, A. Baratoff, H. J. Güntherodt, and T. A. Jung, Chem. Phys. Lett. **417**, 22 (2006).
[28] C. Loppacher, U. Zerweck, L. M. Eng, S. Gemming, G. Seifert, C. Olbrich, K. Morawetz, and M. Schreiber, Nanotechnology **17**, 1568 (2006).
[29] U. Zerweck, C. Loppacher, and L. M. Eng, Nanotechnology **17**, S107 (2006).
[30] B. Such, G. Goryl, S. Godlewski, J. J. Kolodziej, and M. Szymonski, Nanotechnology **19**, 475705 (2008).
[31] T. Glatzel, L. Zimmerli, and E. Meyer, Isr. J. Chem. **48**, 107 (2008).
[32] A. Scarfato, Surf. Sci. **602**, 677 (2008).
[33] C. J. Villagomez, Surf. Sci. **603**, 1526 (2009).
[34] S. A. Burke, W. Ji, J. M. Mativetsky, J. M. Topple, S. Fostner, H. J. Gao, H. Guo, and P. Grütter, Phys. Rev. Lett. **100**, 186104 (2008).
[35] S. A. Burke, J. M. Topple, and P. Grütter, J. Phys.: Condens. Matter **21**, 423101 (2009).
[36] M. Möbus, N. Karl, and T. Kobayashi, J. Cryst. Growth **116**, 495 (1992).
[37] M. Möbus, M. Schreck, and N. Karl, Thin Solid Films **175**, 89 (1989).
[38] D. Schlettwein, A. Back, B. Schilling, T. Fritz, and N. R. Armstrong, Chem. Mater. **10**, 601 (1998).
[39] T. Dienel, S. C. Loppacher, C. B. Mannsfeld, R. Forker, and T. Fritz, Adv. Mater. **20**, 959 (2008).
[40] J. M. Mativetsky, S. A. Burke, S. Fostner, and P. Grütter, Nanotechnology **18**, 105303 (2007).
[41] M. Horn-von Hoegen, Z. Kristallogr. **214**, 591 (1999).
[42] J. Ikonomov, O. Bauer, and M. Sokolowski, Surf. Sci. **602**, 2061 (2008).
[43] E. Le Moal, M. Müller, O. Bauer, and M. Sokolowski, Surf. Sci. **603**, 2434 (2009).
[44] T. Ogawa, K. Kuwamoto, S. Isoda, T. Kobayashia, and N. Karl, Acta Crystallogr., Sect. B: Struct. Sci. **55**, 123 (1999).
[45] R. K. Kirby, T. A. Hahn, and B. D. Rothrock, in *American Institute of Physics Handbook*, edited by D. E. Gray (McGraw-Hill, New York, 1972), p. 4.119.
[46] J. D. H. Donnay, W. P. Mason, and E. A. Wood, in *American Institute of Physics Handbook*, edited by D. E. Gray (McGraw-Hill, New York, 1972), p. 9.1.
[47] F. S. Tautz, Prog. Surf. Sci. **82**, 479 (2007).
[48] L. Kilian, E. Umbach, and M. Sokolowski, Surf. Sci. **600**, 2633 (2006).
[49] S. A. Burke, J. M. Mativetsky, R. Hoffmann, and P. Grütter, Phys. Rev. Lett. **94**, 096102 (2005).
[50] M. Müller, E. Le Moal, and M. Sokolowski (unpublished).
[51] A. Kraft, R. Temirov, S. K. M. Henze, S. Soubatch, M. Rohlfing, and F. S. Tautz, Phys. Rev. B **74**, 041402(R) (2006).
[52] S. A. Burke, J. M. LeDue, J. M. Topple, S. Fostner, and P. Grütter, Adv. Mater. **21**, 2029 (2009).